Journal of Materials Chemistry

Cite this: J. Mater. Chem., 2012, 22, 11107

www.rsc.org/materials

PAPER

Columnar assembly and successive heating of colloidal 2D nanomaterials on graphene as an efficient strategy for new anode materials in lithium ion batteries: the case of In_2S_3 nanoplates†

Jaewon Choi,[a] Jaewon Jin,[a] Jeho Lee,[a] Ji Hoon Park,[a] Hae Jin Kim,[b] Dong-Hwa Oh,[c] Joung Real Ahn*[c] and Seung Uk Son*[a]

Received 15th February 2012, Accepted 29th March 2012
DOI: 10.1039/c2jm30949a

This study shows that heat-treatment of colloidal inorganic nanoplates with columnar assembly under argon is a good strategy for development of anode materials. The heating of colloidal In_2S_3 nanoplates under argon resulted in the formation of film-like materials through interconnection of plates in a side by side manner. When the columnarly assembled colloidal In_2S_3 plates were heated at 400 °C under argon for 2 hours *on graphene*, more efficient anode materials with smaller diameters were obtained. Interestingly, the heat-treated columnarly assembled In_2S_3 plates on graphene had a layered structure, which was attributed to the possible existence of carbon materials between plates formed by the heat-treatment of surfactants under argon. The resultant graphene–In_2S_3 composites showed enhanced discharge capacities, up to 716–837 mA h g^{-1}, as well as excellent stabilities. In addition, the materials showed promising coulombic efficiencies and rate performances. We believe that, based on the strategy in this work, diverse graphene–inorganic nanomaterial composites with a layered structure can be prepared and applied as new anode materials in lithium ion batteries.

Introduction

As sustainable energy became an important issue, related energy storage devices have attracted great attention of scientists.[1] Currently, the lithium ion battery (LIB) is one of the most promising energy storage devices for electrical energy.[1,2] For further improvement of the energy storage capacity and stability of LIB, extensive exploration for superior electrode materials has been actively conducted.[2] In addition to zerovalent inorganic materials, diverse metal oxides and chalcogenides have been applied as electrode materials.[2]

Recently, with the rise of graphene as a new conductive platform,[3] graphene composites of the diverse inorganic materials have been prepared[4] and showed improved capacities and stabilities as electrode materials for LIB.[5] Usually, the graphene composites are prepared *via* wet chemical processes using graphene oxide obtained from the Hummers method.[6] Especially, for efficient formation of composites between the reduced graphene oxide flakes and inorganic materials, diverse size- and shape-controlled colloidal inorganic nanomaterials can be utilized in wet chemical processes in solution.

During the last several decades, there has been great progress in size and shape controlled synthesis of colloidal nanomaterials.[7] Among the diverse colloidal nanomaterials, two dimensional (2D) materials such as nanoplates, nanodiscs and nanoribbons have attracted significant attention of scientists.[8] Especially, as graphene showed interesting physical properties, graphene-like ultrathin inorganic nanomaterials have attracted new or renewed attention of scientists.[8] In addition to physical synthetic approaches such as chemical vapour deposition,[9] the wet-chemical colloidal approach resulted in the diverse 2D inorganic nanomaterials.[7,8] For example, the kinetically controlled growth using diverse surfactants induced 2D shape evolution of materials. Interestingly, 2D nanomaterials, even with an isotropic cubic-phase, were successfully prepared *via* the assembly of precursors and the successive kinetically controlled growth of materials.[10] In these cases, the surfactants interact selectively with the growing crystalline planes and inhibit the growth of certain crystalline planes, resulting in 2D shape evolution of materials.

One of the interesting behaviors of colloidal 2D nanomaterials is their facile columnar assembly through van der Waals interaction among surfactants on a surface.[8] Our research group has developed diverse colloidal 2D nanomaterials showing columnar packing between materials.[10,11] With this behavior in mind, we

[a]*Department of Chemistry, Department of Energy Science, Sungkyunkwan University, Suwon 440-746, Korea. E-mail: sson@skku.edu; Fax: +82-031-290-4572; Tel: +82-031-299-5932*
[b]*Korea Basic Science Institute, Daejeon 350-333, Korea*
[c]*Department of Physics and SAINT, Sungkyunkwan University, Suwon 440-746, Korea. E-mail: jrahn@skku.edu*

† Electronic supplementary information (ESI) available: Additional TEM, HR-TEM and SEM images and electrochemical characterization of cells. See DOI: 10.1039/c2jm30949a

thought that the ideal materials having a layered structure and a relatively small diameter can be achieved for efficient lithium insertion. It was reasoned that the layered structure and a small diameter of materials will induce not only enhanced stability due to the structural flexibility, but also high capacity due to enhanced active sites for Li insertion. Thus, ultimately, enhanced storage performance in lithium ion batteries can be expected. As revealed in Scheme 1, columnar assembly and successive heating of the colloidal nanoplates can induce growth in the normal direction to a basal plane. Especially, it was expected that the heating of colloidal plates having surfactants on the surface under argon will result in the incorporation of carbon materials between plates, which will improve the conductivity of materials.

Experimental section

Apparatus

Transmission electron microscopy (TEM) and high resolution TEM images were obtained using a JEOL 2100F unit operated at 200 kV. Samples for TEM were prepared on a copper grid by drop-casting methylene chloride and hexane solutions of the nanomaterials. The scanning electron microscopy (SEM) images in the ESI† were taken by FE-SEM (JSM6700F). Powder X-ray diffraction (PXRD) patterns were obtained using a Rigaku MAX-2200 and filtered Cu-Kα radiation. X-ray photoelectron spectroscopy (XPS) was conducted using a Thermo VG and monochromatic Al-Kα radiation.

Synthetic procedure for colloidal ultrathin In_2S_3 nanoplates used in this study

The β-In_2S_3 nanoplates were prepared by the modified synthetic method reported by our group.[11a] Under a vacuum, oleylamine (9 mL) was heated at 100 °C for 3 hours to remove water. In a 50 mL two neck Schlenk flask, anhydrous $InCl_3$ (0.20 g, 0.90 mmol) was dissolved in well-dried oleylamine (7 mL) under argon, heated at 100 °C for 1 hour, then cooled to room temperature. In a 10 mL flame-dried vial, sulfur powder (44 mg, 1.4 mmol) was dissolved in well-dried oleylamine (2 mL). Two solutions were combined and the reaction temperature was rapidly increased to 215 °C. After aging at 215 °C for an additional 1.5 hours, the reaction mixture was cooled to room temperature. Addition of the excess methanol resulted in the precipitates which were retrieved by centrifugation. The resultant bright yellow powder was dried under a vacuum.

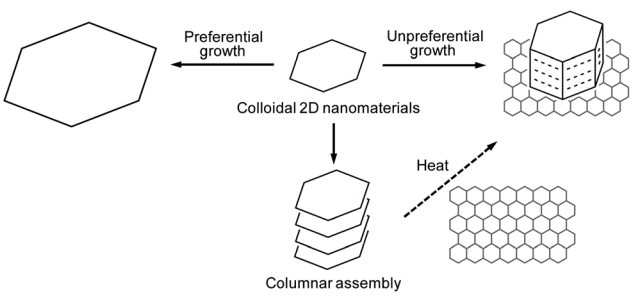

Scheme 1 The formation of nanomaterials with a layered structure *via* columnar assembly and successive heating of colloidal nanoplates under argon.

Synthetic procedure for composites

Graphene oxide flakes were prepared from graphite by the Hummers method.[6a] Graphene oxide (30 mg for **H-GIS-1**, 20 mg for **H-GIS-2**) was well-dispersed in methanol (25 mL). After addition of In_2S_3 nanoplates (30 mg for **H-GIS-1**, 40 mg for **H-GIS-2**), the solution was sonicated for 1 day. The In_2S_3 plates formed columnar assembly in powder form and were not disassembled in methanol. Through sonication, the assembled In_2S_3 columns were gradually sliced into short ones. Then, hydrazine monohydrate (0.40 mL, 8.2 mmol) was added to the solution.[12] The reaction mixture was heated at 80 °C for 3 hours, which induced the formation of black precipitates. After being separated from the solution by centrifugation, the composites were washed with acetone three times, dried under a vacuum and heated at 400 °C for 2 hours under argon.

Electrochemical studies

For fabrication of the working electrode, the In_2S_3–graphene composites (80 mg), Super P carbon black (10 mg) and polyvinylidene fluoride binder (10 mg) were mixed in *N*-methylpyrrolidone (NMP). After coating the copper foil with this mixture, the electrode was dried under a vacuum at 120 °C overnight. Cell tests were performed using coin-type half cells (CR2016 type) with Li metal as the counter-electrode and 1 M $LiPF_6$ in ethylene carbonate–diethyl carbonate (1 : 1, v/v) as the electrolyte. The discharge–charge cycle tests were performed using a WBCS3000 automatic battery cycler system.

Results and discussion

During the last decade, our research group has continued the development of the synthetic method for diverse 2D nanomaterials.[10,11] For example, colloidal ultrathin In_2S_3, TiS_2, Sb_2S_3, Ga_2O_3, $SnSe_2$, $Cu_{2-x}Se$, and Rh nanomaterials have been prepared.[10,11] Thus, to apply the synthetic strategy in Scheme 1, we selected the colloidal ultrathin In_2S_3 nanoplates which were previously reported by our group.[11a] It is noteworthy that the prepared In_2S_3 has a defect spinel structure which can accommodate diverse cationic metals.[13] For example, Eu^{3+}, Mn^{2+} and Co^{2+} ions were incorporated into In_2S_3 and the change of optical properties was reported.[14] In addition, the Li insertion into In_2S_3 materials was characterized[15] and their application as anode materials for LIB has been reported.[13c] However, in the literature, a notorious problem with In_2S_3, as anode materials in LIB was the fast fading of storage capacity.[13c] Thus, enhancement of stability and capacity of In_2S_3 materials was a quite challenging goal in our work.

The colloidal ultrathin β-In_2S_3 nanoplates (**IS**) with 34 nm diameter and ~0.80 nm thickness were prepared; they showed conventional columnar assembly behavior, as shown in Fig. 1a and b and S1 in the ESI†. According to the TEM analysis, almost all the plates were in an assembled state. The average interplate distance (between two centers of thickness) was ~2.3 nm (Fig. 1b). The ~1.5 nm space, with a low contrast between plates, indicates the existence of insulating surfactants on the surfaces of

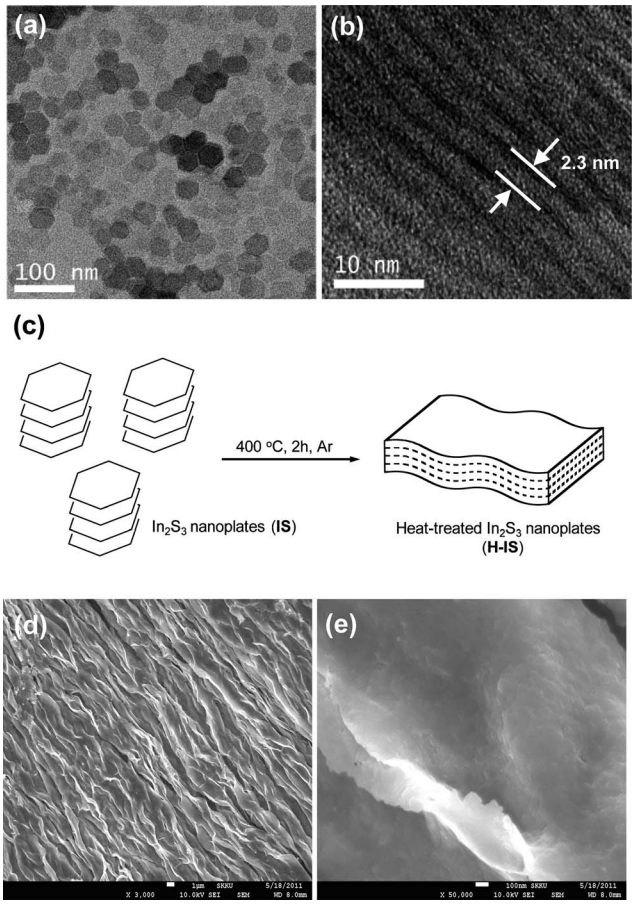

Fig. 1 (a and b) TEM images of the colloidal In_2S_3 nanoplates (**IS**), (c) cartoon of formation of a film-like big plate of In_2S_3 (**H-IS**) *via* heating of columnarly assembled In_2S_3 nanoplates and (d and e) their SEM images.

plates. These colloidal plates showed very poor Li-storage performance possibly due to low conductivity (see the part of electrochemical tests). Thus, to develop better anode materials in lithium ion batteries, the columnarly assembled colloidal In_2S_3 nanoplates were heated at 400 °C for 2 hours *under argon* (**H-IS**). It was expected that layered materials with a columnar shape and relatively small diameter (~34 nm) would be formed. However, as shown in Fig. 1c–e, the plates were interconnected in a side by side manner to form relatively large and undulating film-like materials. This means that although the colloidal In_2S_3 nanoplates were columnarly assembled, they still have a strong preference for planar growth of plates. It can be reasoned that the sides of In_2S_3 plates were less efficiently blocked by surfactants than the up and down faces of plates.

Interestingly, the side view of pieces of film-like materials (**H-IS**) shows that they were formed *via* packing of plates and that they have layers (Fig. S2 in the ESI†). PXRD analysis showed that the resultant materials maintained the original β-In_2S_3 phase (Fig. 3a). Considering the color change from the original bright yellow to black, it was speculated that the surfactants turned into carbon materials between plates. The elementary analysis showed that 3.0 wt% C remained in the heat-treated In_2S_3 nanoplates (**H-IS**) and the wt% ratio of C to H increased from 6.1 (experimental value of **IS**, *cf.* the theoretical value of oleylamine, 5.8) to 48.

A similar heat-treatment was conducted for columnarly assembled In_2S_3 nanoplates on graphene. The In_2S_3–graphene composites (**GIS**) were heated at 400 °C for 2 hours *under argon*[16] (see Experimental section for detailed procedure). Depending on the relative amount of In_2S_3 against graphene with 1 : 1 and 2 : 1 ratios, the two heat-treated composites (**H-GIS-1** and **H-GIS-2**) were prepared respectively.

The **H-GIS** composites were investigated by TEM, HR-TEM and SEM. As shown in Fig. 2a and S3†, the locally assembled In_2S_3 nanomaterials were observed over graphene. Careful analysis on the formed materials by HR-TEM revealed the materials to have a layered structure (Fig. 2b). Compared with

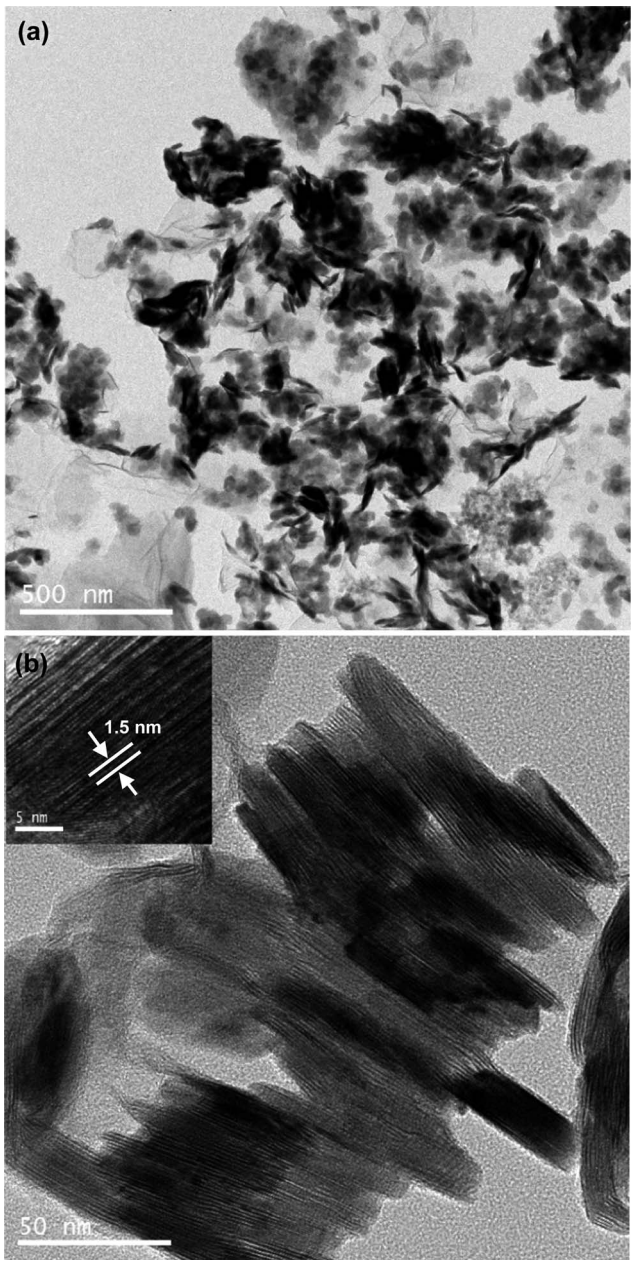

Fig. 2 (a) TEM image of In_2S_3 materials on graphene (**H-GIS-2**), prepared *via* the heating of columnarly assembled In_2S_3 nanoplates in graphene and (b) their HR-TEM images.

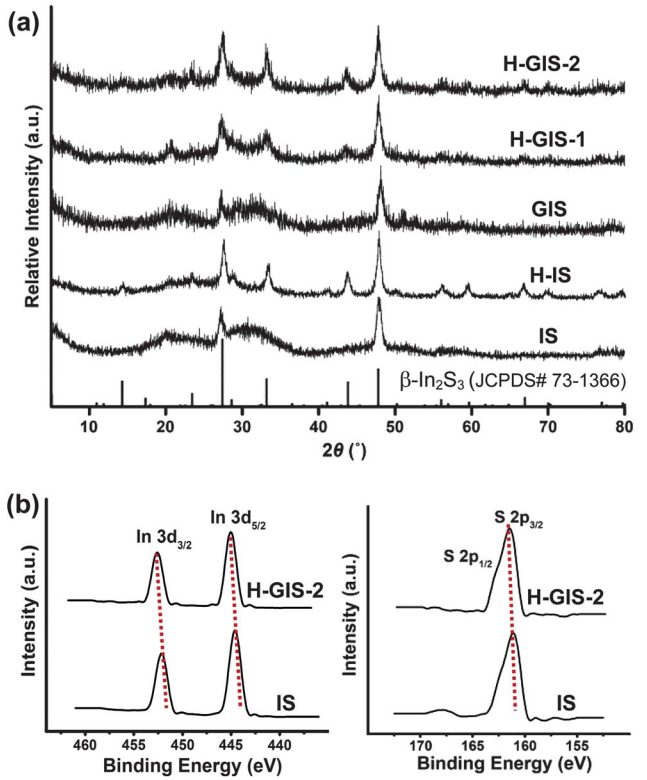

Fig. 3 (a) Powder X-ray diffraction patterns of colloidal In_2S_3 nanoplates (**IS**), heat-treated In_2S_3 nanoplates (**H-IS**), composites of graphene and In_2S_3 nanoplates (**GIS**), heat-treated graphene composites of In_2S_3 nanoplates (**H-GIS-1**, **H-GIS-2**) and (b) comparison of XPS spectra of **H-GIS-1** and **IS**.

a case without the use of graphene (**H-IS**) in Fig. 1d and e, the interconnection of nanoplates in a side by side manner was significantly suppressed. It was reasoned that the existence of a graphene platform limited the side by side aggregation of the columnarly assembled nanoplates and hence, induced the locally isolated assembled materials. The successive heat-treatment under argon resulted in the columnarly packed materials with layers. The interlayer distance of In_2S_3 materials in **H-GIS** was reduced from that of the original colloidal In_2S_3 nanoplates, ~2.3 nm to ~1.5 nm (the inset in Fig. 2b). The vivid layer structure in the HR-TEM image in Fig. 2b is attributed to the existence of carbon materials between layers.[17] According to the HR-TEM analysis, certain parts of **H-GIS** showed the formation of a nearly complete crystal lattice by the oriented attachment of plates (Fig. S4 in the ESI†). The distance between the crystal planes, located in the vertical direction of the basal plane, was clearly measured as 0.38 nm, which is close to the (200) plane of tetragonal β-In_2S_3 (JCPDS# 73-1366).[13]

The formation of the larger crystalline domains in **H-GIS** by heating, compared with ultrathin In_2S_3 building blocks, was further verified by PXRD and XPS studies. The original colloidal In_2S_3 nanoplates (**IS**) showed two main peaks at 27 and 48° in the PXRD pattern, which correspond to the (109) and (2212) crystal planes of the tetragonal β-In_2S_3 (Fig. 3). Another two major peaks from (0012) and (309) crystal planes at 33 and 43° respectively were suppressed due to the ultrathin nature of **IS**. Heating of the colloidal In_2S_3 nanoplates (**H-IS**) resulted in the appearance of these two peaks. The graphene composites of In_2S_3 nanoplates without heating (**GIS**) showed a very similar PXRD pattern with the original colloidal In_2S_3 nanoplates (**IS**), verifying the absence of decomposition of In_2S_3 nanoplates during the reduction process of graphene oxide by hydrazine. The heat treatment of **GIS** resulted in the gradual appearance of two peaks from (0012) and (309) planes with the increased amount of In_2S_3 materials, indicating the formation of the larger crystalline domains by heat-treatment. The electronic surroundings of In and S in **H-GIS** were compared with those in **IS** by XPS (Fig. 3b). The In $3d_{5/2}$ and S $2p_{3/2}$ peaks of **H-GIS** appeared at 444.9 and 161.3 eV respectively and were shifted slightly to a higher binding energy, compared with those of **IS** at 444.4 and 160.9 eV respectively. The binding energy of In $3d_{5/2}$ of **H-GIS** was closer to the value (444.8 eV) of bulky In_2S_3 materials than to that of **IS**.[18]

The obtained materials were tested as anode materials in lithium ion batteries. Using five materials (**IS**, **H-IS**, **H-GIS-1**, **H-GIS-2** and reduced graphene oxides), the coin-type electrochemical cells were fabricated respectively (see Experimental section for details of the procedure). The cells were discharged from an open-circuit voltage to 1 mV and then, cycled between 1 mV and 3.0 V at a current density of 50 mA g^{-1}. Fig. 4a shows the discharge capacities (average values of three runs) depending on the charge–discharge cycles at the 50 mA g^{-1} current density.

First, **IS** showed very poor discharge capacity and cycling stability. The discharge capacities were rapidly decreased from 300 mA h g^{-1} at the second cycle to 62 mA h g^{-1} after 30 cycles. This observation is very similar to results in the literature.[13c] The poor electrochemical performance of **IS** can be attributed to the existence of insulating organic surfactant on the surfaces of In_2S_3 nanoplates as well as the absence of an interlayer space due to the ultrathin nature. In comparison, **H-IS** showed significantly increased discharge capacity and improved cycling stability. At the second cycle, 582 mA h g^{-1} discharge capacity was observed and, after 30 cycles, the discharge capacity was gradually reduced to 481 mA h g^{-1}. **H-GIS** showed the most promising cell performance among the materials tested in this work. In the case of **H-GIS-1**, at the second cycle, a 718 mA h g^{-1} discharge capacity was observed and even after 30 cycles, the 716 mA h g^{-1} discharge capacity was maintained. In the case of **H-GIS-2**, the discharge capacity was further increased to 841 mA h g^{-1} at the second cycle and 837 mA h g^{-1} after 30 cycles. Coulombic efficiencies reached above 97% after 10 cycles (Fig. 4a and S5 in the ESI†). Not only the discharge capacities but also the stabilities of these **H-GIS** dramatically improved, compared with **IS** and **H-IS**. The enhanced discharge capacity of **H-GIS**, compared with **H-IS**, can be attributed to the increased active sites due to the shape effect, as explained in Fig. 4b, as well as increased conductivity by graphene. It is well recognized that the introduction of a structurally flexible space in electrode materials enhances stability in cell cyclings.[19] Thus, the excellent stability of **H-GIS** can be attributed to a layered structure with structural flexibility, originated from the possible existence of carbon materials between layers (Fig. 2b), in addition to the well-documented buffering role of graphene.[5]

Fig. 4c shows the charge–discharge curves of **H-GIS-2**, in which the shoulder was observed at 1.2 V (*vs.* Li/Li^+) in reversible discharge curves (Fig. S6 in the ESI† for charge–discharge curves

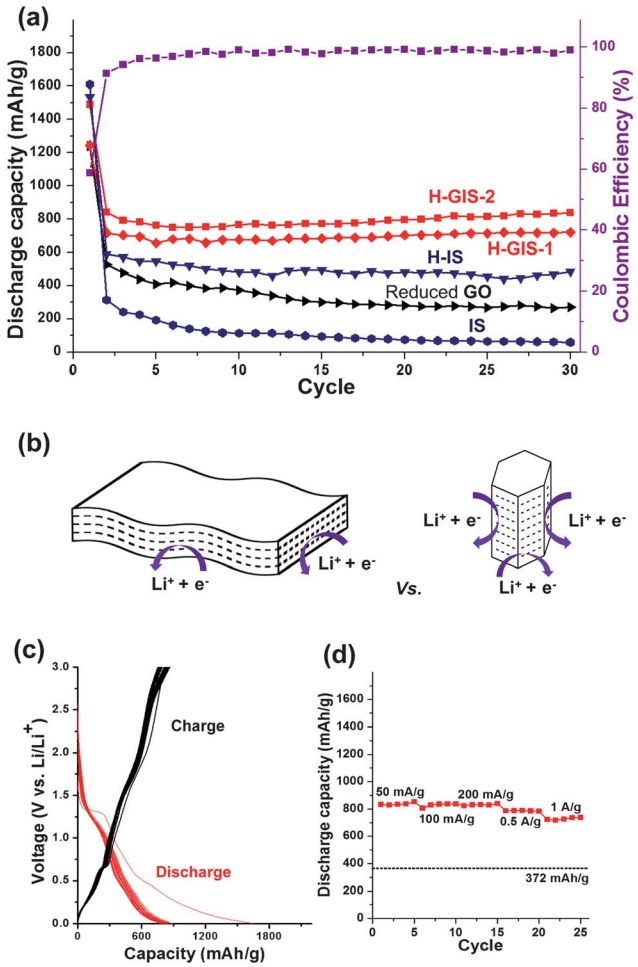

Fig. 4 (a) Discharge capacities (average values of three runs at the 50 mA g^{-1} current density) dependent on cycle numbers of **IS**, reduced graphene oxides (GOs), **H-IS**, **H-GIS-1** and **H-GIS-2** and coulombic efficiencies of **H-GIS-2** (violet colored curve), (b) cartoon of Li insertion to In_2S_3 materials in **H-IS** (left) and **H-GIS** (right), (c) selected charge–discharge curves from three runs obtained at the 50 mA g^{-1} current density and (d) rate performance of **H-GIS-2**.

of **H-GIS**, **H-IS**, **IS** and reduced graphene oxide). Basically, discharge curves of **H-GIS** were very similar to those of In_2S_3-based anode materials in the literature.[13a] It is noteworthy that, in control experiments, graphene which was prepared *via* the same experimental procedures for **H-GIS**, without the use of In_2S_3 materials, showed a 271 mA h g^{-1} discharge capacity after 30 cycles and no shoulder peaks at 1.2 V (*vs.* Li/Li^+) in reversible discharge curves (Fig. S6 in the ESI†). As shown in Fig. 4d, **H-GIS-2** showed excellent rate performance with the 836 and 826 mA h g^{-1} discharge capacities at 100 and 200 mA g^{-1} current densities. Even at 0.5 and 1 A g^{-1} current densities, **H-GIS-2** maintained 787 and 738 mA h g^{-1} discharge capacities respectively, which are significantly higher than the discharge capacity (372 mA h g^{-1}) of commercialized graphite.

Conclusions

This study shows that heat-treatment of colloidal 2D nanomaterials with columnar assembly under argon is a good strategy for the development of anode materials. The heating of colloidal In_2S_3 nanoplates resulted in the formation of film-like materials through interconnection of plates in a side by side manner. When the columnarly assembled colloidal In_2S_3 plates were heated at 400 °C for 2 hours on graphene, more efficient anode materials with smaller diameters were obtained. Interestingly, the heat-treated columnarly assembled In_2S_3 plates in graphene had a layered structure, which was attributed to the possible existence of carbon materials between plates formed by heat-treatment of surfactant under argon. The heat-treated graphene–In_2S_3 composites showed enhanced discharge capacities, up to 716–837 mA h g^{-1}, as well as excellent stabilities. In addition, the materials showed promising coulombic efficiencies and rate performances. We believe that, based on the strategy in this work, diverse graphene–inorganic nanomaterial composites with a layered structure can be prepared and applied as new anode materials in lithium ion batteries.

Acknowledgements

This work was supported by grants NRF-2009-0064488 through the National Research Foundation of Korea funded by the Ministry of Education, Science and Technology. JHP thanks for grants NRF-2011-0031392 (Priority Research Centers Program) and R31-2008-10029 (WCU program). HJK thanks for KBSI grants P30402 and Hydrogen Energy R&D Center, a 21st century Frontier Program.

Notes and references

1 Review: F. Cheng, Z. Tao, J. Liang and J. Chen, *Chem. Mater.*, 2008, **20**, 667.
2 Reviews: (*a*) P. G. Bruce, B. Scrosati and J.-M. Tarascon, *Angew. Chem., Int. Ed.*, 2008, **47**, 2930; (*b*) M. S. Whittingham, *Dalton Trans.*, 2008, 5424.
3 K. S. Novoselov, A. K. Geim, S. V. Morozov, D. Jiang, S. Zhang, V. Dubonos, I. V. Grigorieva and A. A. Firsov, *Science*, 2004, **306**, 666.
4 Reviews: (*a*) X. An and J. C. Yu, *RSC Adv.*, 2011, **1**, 1426; (*b*) P. V. Kamat, *J. Phys. Chem. Lett.*, 2010, **1**, 520.
5 (*a*) S.-M. Paek, E. Yoo and I. Honma, *Nano Lett.*, 2009, **9**, 72; (*b*) Y. Li and Y. Wu, *J. Am. Chem. Soc.*, 2009, **131**, 5851; (*c*) G. Wang, B. Wang, X. Wang, J. Park, S. Dou, H. Ahn and K. Kim, *J. Mater. Chem.*, 2009, **19**, 8378; (*d*) D. Wang, D. Choi, J. Li, Z. Yang, Z. Nie, R. Kou, D. Hu, C. Wang, L. V. Saraf, J. Zhang, I. A. Aksay and J. Liu, *ACS Nano*, 2009, **3**, 907; (*e*) F. Ji, Y.-L. Li, J.-M. Feng, D. Su, Y.-Y. Wen, Y. Feng and F. Hou, *J. Mater. Chem.*, 2009, **19**, 906; (*f*) G. Zhou, D.-W. Wang, F. Li, L. Zhang, N. Li, Z.-S. Wu, L. Wen, G. Q. Lu and H.-M. Cheng, *Chem. Mater.*, 2010, **22**, 5306; (*g*) S.-L. Chou, J.-Z. Wang, M. Choucair, H.-K. Liu, J. A. Stride and S.-X. Dou, *Electrochem. Commun.*, 2010, **12**, 303; (*h*) P. V. Kamat, *J. Phys. Chem. Lett.*, 2010, **1**, 520; (*i*) H. Wang, L.-F. Cui, Y. Yang, H. S. Casalongue, J. T. Robinson, Y. Liang, Y. Cui and H. Dai, *J. Am. Chem. Soc.*, 2010, **132**, 13978; (*j*) J. Liu, S. Fu, B. Yuan, Y. Li and Z. Deng, *J. Am. Chem. Soc.*, 2010, **132**, 7279; (*k*) C. Zhong, J. Wang, Z. Chen and H. Liu, *J. Phys. Chem. C*, 2011, **115**, 25115; (*l*) Y. Zou, J. Kan and Y. Wang, *J. Phys. Chem. C*, 2011, **115**, 20747.
6 (*a*) W. Hummers and R. Offeman, *J. Am. Chem. Soc.*, 1958, **80**, 466; (*b*) S. Stankovich, D. A. Dikin, R. D. Piner, K. A. Kohlhaas, A. Kleinhammes, Y. Jia, Y. Wu, S. T. Nguyen and R. S. Ruoff, *Carbon*, 2007, **45**, 1558.
7 D. V. Talapin, J.-S. Lee, M. V. Kovalenko and E. V. Shevchenko, *Chem. Rev.*, 2010, **110**, 389.
8 Selected examples: (*a*) D. Kong, W. Dang, J. J. Cha, H. Li, S. Meister, H. Peng, Z. Liu and Y. Cui, *Nano Lett.*, 2010, **10**, 2245; (*b*) D. D. Vaughn, S.-I. In and R. E. Schaak, *ACS Nano*, 2011, **5**, 8852;

(*c*) F. Zhao, M. Yuan, W. Zhang and S. Gao, *J. Am. Chem. Soc.*, 2006, **128**, 11758; (*d*) Y. C. Cao, *J. Am. Chem. Soc.*, 2004, **126**, 7456; (*e*) M. B. Sigman, A. Ghezelbash, T. Hanrath, A. E. Saunders, F. Lee and B. A. Korgel, *J. Am. Chem. Soc.*, 2003, **125**, 16050.

9 Selected examples: (*a*) S. S. Garje, D. J. Eisler, J. M. Ritch, M. Afzaal, P. O'brien and T. Chivers, *J. Am. Chem. Soc.*, 2006, **128**, 3120; (*b*) K.-J. Wang, G.-D. Li, J.-X. Li, Q. Wang and J.-S. Chen, *Cryst. Growth Des.*, 2007, **7**, 2265; (*c*) W. Dang, H. Peng, H. Li, P. Wang and Z. Liu, *Nano Lett.*, 2010, **10**, 2870.

10 K. Jang, H. J. Kim and S. U. Son, *Chem. Mater.*, 2010, **22**, 1273.

11 (*a*) K. H. Park, K. Jang and S. U. Son, *Angew. Chem., Int. Ed.*, 2006, **45**, 4608; (*b*) K. H. Park, J. Choi, H. J. Kim, D.-H. Oh, J. R. Ahn and S. U. Son, *Small*, 2008, **4**, 945; (*c*) K. H. Park, J. Choi, H. J. Kim, J. B. Lee and S. U. Son, *Chem. Mater.*, 2007, **19**, 3861; (*d*) J. Xu, K. Jang, I. G. Jung, H. J. Kim, D.-H. Oh, J. R. Ahn and S. U. Son, *Chem. Mater.*, 2009, **21**, 4347; (*e*) J. Choi, N. Kang, H. Y. Yang, H. J. Kim and S. U. Son, *Chem. Mater.*, 2010, **22**, 3586; (*f*) J. Choi, J. Jin, I. G. Jung, J. M. Kim, H. J. Kim and S. U. Son, *Chem. Commun.*, 2011, **47**, 5241.

12 S. Stankovich, D. A. Dikin, R. D. Piner, K. A. Kohlhaas, A. Kleinhammes, Y. Jia, Y. Wu, S. T. Nguyen and R. S. Ruoff, *Carbon*, 2007, **45**, 1558.

13 (*a*) L.-Y. Chen, Z.-D. Zhang and W.-Z. Wang, *J. Phys. Chem. C*, 2008, **112**, 4117; (*b*) M. A. Franzman and R. L. Brutchey, *Chem. Mater.*, 2009, **21**, 1790; (*c*) L. Liu, H. Liu, H.-Z. Kou, Y. Wang, Z. Zhou, M. Ren, M. Ge and X. He, *Cryst. Growth Des.*, 2009, **9**, 113; (*d*) B. G. Kumar and K. Muralidharan, *J. Mater. Chem.*, 2011, **21**, 11271; (*e*) J. Ning, K. Men, G. Xiao, L. Zhao, L. Wang, B. Liu and B. Zou, *J. Colloid Interface Sci.*, 2010, **347**, 172; (*f*) F. Ye, C. Wang, G. Du, X. Chen, Y. Zhong and J. Z. Jiang, *J. Mater. Chem.*, 2011, **21**, 17063; (*g*) S. Rengaraj, S. Venkataraj, C. Tai, Y. Kim, E. Repo and M. Sillanapää, *Langmuir*, 2011, **27**, 5534.

14 (*a*) W. Chen, J.-O. Bovin, A. G. Joly, S. Wang, F. Su and G. Li, *J. Phys. Chem. B*, 2004, **108**, 11927; (*b*) A. Datta, S. Gorai and S. Chaudhuri, *J. Nanopart. Res.*, 2006, **8**, 919; (*c*) A. Datta, D. Ganguli and S. Chaudhuri, *J. Mater. Res.*, 2008, **23**, 917.

15 A. Kulińska, M. Uhrmacher, R. Dehryvère, A. Lohstroh, H. Hofsäss, K. P. Lieb, A. Picard-Garcia and J.-C. Jumas, *J. Solid State Chem.*, 2004, **177**, 109.

16 A heat-treatment of the composites at 700 °C for 2 hours resulted in a severe aggregation of In_2S_3 materials with a poor storage capacity.

17 In XPS analysis, a trace amount of nitrogen was detected.

18 J. F. Moulder, W. F. Stickle, P. E. Sobol and K. D. Bomben, *Handbook of X-Ray Photoelectron Spectrscopy*, Physical Elentronics, Inc., 1992.

19 Selected examples: (*a*) J. S. Chen, T. Zhu, X. H. Yang, H. G. Yang and Z. W. Lou, *J. Am. Chem. Soc.*, 2010, **132**, 13162; (*b*) Y. Sun, X. Hu, W. Luo and Y. Huang, *ACS Nano*, 2011, **5**, 7100; (*c*) L. Wu, H. Yao, B. Hu and S.-H. Yu, *Chem. Mater.*, 2011, **23**, 3946; (*d*) B. Wang, J. S. Chen, H. B. Wu, Z. Wang and X. W. Lou, *J. Am. Chem. Soc.*, 2011, **133**, 17146.

